IOP Publishing Smart Materials and Structures
Smart Mater. Struct. 24 (2015) 025012 (13pp) doi:10.1088/0964-1726/24/2/025012

Flexible fiber batteries for applications in smart textiles

Hang Qu[1], Oleg Semenikhin[2] and Maksim Skorobogatiy[1]

[1] Department of Engineering Physics, Ecole Polytechnique de Montréal, C.P. 6079, succ. Centre-ville, Montréal, (Québec), Canada, H3C 3A7, Canada
[2] Department of Chemistry, University of Western Onataria, London, Ontario, Canada, N6A 5B7, Canada

E-mail: maksim.skorobogatiy@polymtl.ca

Received 18 June 2014, revised 22 November 2014
Accepted for publication 25 November 2014
Published 16 December 2014

Abstract

In this paper, we demonstrate flexible fiber-based Al–NaOCl galvanic cells fabricated using fiber drawing process. Aluminum and copper wires are used as electrodes, and they are introduced into the fiber structure during drawing of the low-density polyethylene microstructured jacket. NaOCl solution is used as electrolyte, and it is introduced into the battery after the drawing process. The capacity of a 1 m long fiber battery is measured to be ~10 mAh. We also detail assembly and optimization of the electrical circuitry in the energy-storing fiber battery textiles. Several examples of their applications are presented including lighting up an LED, driving a wireless mouse and actuating a screen with an integrated shape-memory nitinol wire. The principal advantages of the presented fiber batteries include: ease of fabrication, high flexibility, simple electrochemistry and use of widely available materials in the battery design.

Keywords: smart textiles, fiber battery, fiber battery textile

(Some figures may appear in colour only in the online journal)

1. Introduction

With the rapid advances in new materials and driven by the need to increase the value of conventional textiles, research into smart textiles has recently flourished [1–4]. Generally, textiles are considered 'smart' if they can respond to various stimulus, such as mechanical, thermal, chemical, electrical, and magnetic. In many cases 'smart' textiles have to host various electronics that should be seamlessly and reliably integrated into a flexible textile matrix. In the early prototypes, conventional rigid electronic was directly attached to a textile, which typically resulted in clumsy prototypes and unreliable performance. From the early on it was noted that the fundamental incompatibility between the rigid electronic components and a soft textile matrix creates a significant barrier for spreading of this promising technology into wearable applications. This problem motivated much of the recent research efforts into the development of soft electronics, sensors and actuators for applications in the truly wearable smart textiles. Needless to say that to drive these functional components one needs an efficient, lightweight and flexible battery source. Ideally, such a source would be directly in the form of a fiber that can be naturally integrated into smart textiles during weaving.

To date, a number of lithium-ion fiber batteries have been demonstrated. In 2003, Neudecker *et al* [5] have proposed that lithium-ion batteries can be fabricated by sequential vacuum deposition of battery-component thin-layers (such as in sequence of anode, electrolyte, cathode layer) on fiber substrates. These fiber batteries could be embedded in an adhesive matrix to constitute a battery ribbon. However, the fabrication of these fiber batteries requires complicated vacuum deposition techniques including magnetron sputtering and electron-beam evaporation. In 2005, Wang *et al* [6] developed fiber batteries based on intrinsically conducting polymers. To fabricate the batteries, polypyrrole-hexafluorophosphate (PPy/PF_6) is first coated on a platinum (Pt) wire as the cathode. Then, the cathode wire is inserted into a hollow-core polyvinylidene fluoride (PVDF) membrane wrapped by the anode wire which is a Pt wire coated by polypyrrole-polystyrenesulfonate (PPy-PSS). Finally, the whole structure is immersed in a glass vial filled with 1 M ($1\ M = 1\ mol\ L^{-1}$) lithium hexafluorophosphate ($LiPF_6$) electrolyte solution. Battery capacities on the order of 10

milliampere hour per gram (mAh g^{-1}) over 30 cycles were observed. Later, the same group [7] also used single-wall carbon nanotubes (CNTs) to replace PPy-PPS for the fabrication of anode. The capacities were thus improved to ~20 mAh g^{-1}. Note that both of these fiber batteries should be immersed in $LiPF_6$ organic solutions to operate, which makes them unsuitable for smart textile applications. In 2012, LG Chem. Ltd [8] reported a cable-type flexible lithium-ion battery which is fabricated by encapsulating a hollow-spiral tin–nickel (Sn–Ni) anode, and a lithium cobalt oxide ($LiCoO_2$) composite cathode within a heat-shrinkable polymer tube. A poly(ethylene terephthalate) (PET) nonwoven layer was wound on the anode as a separator, and 1 M $LiPF_6$ was injected into the battery cable as electrolyte. This cable-type battery has a linear capacity of ~1 milliampare hour per centimeter (mAh cm^{-1}). Recently, Peng and coworkers [9] demonstrated a flexible fiber-shaped lithium-ion battery by winding, onto a polymer substrate fiber, an anode yarn and a cathode yarn with a separator layer in between. The anode and cathode yarn were fabricated from CNT /lithium titanium oxide ($Li_4Ti_5O_{12}$) composite and CNT/lithium manganate ($LiMn_2O_4$) composite, respectively; and 1 M $LiPF_6$ was used as electrolyte. This battery achieved a capacity of 138 mAh g^{-1} when discharging at 0.01 mA. Later, the same group [10] replaced the lithium-salt cathode yarn by a CNT/silicon (Si) composite yarn, and reported a capacity of ~100 mAh g^{-1} at 1 C-rate. Besides, Kim *et al* [11] demonstrated a 'layer-built' lithium ribbon-type battery which is fabricated by stacking $LiFePO_4$ cathodes and amorphous-silicon-film anodes inside a polymer tube. PVDF membranes containing 1 M $LiPF_6$ were used as separators. Experimental results showed that this ribbon-type (2.4 mm wide, 1 mm thick) battery had a discharge capacity of 166.4 mAh g^{-1} at 0.5 C-rate with flat charge/discharge characteristics and good cycling efficiency.

The above-mentioned fiber or cable type batteries are all lithium-ion batteries that normally require complicated synthesis of battery components, complex battery assembly in the controlled environment, and use of toxic organic solvents. Alternatively, fiber batteries could be implemented using a simple galvanic configuration. For example, Yu *et al* [12] demonstrated a fiber-type zinc–carbon battery based on carbon fiber electrodes. In this design, a zinc wire (or a zinc-coated carbon fiber) was used as anode and a manganese dioxide (MnO_2)-coated carbon fiber was used as cathode. The cathode and anode fibers were separated by a spacer, and then sealed into a flexible capillary fiber filled with ammonium chloride (NH_4Cl) electrolyte solution. This fiber battery showed high flexibility and had a capacity of 158 mAh g^{-1}. However, the mass production of this fiber battery could be problematic, since the electrode wires need to be manually inserted into the capillary fiber. We also note that supercapacitors could also be fabricated in the fiber form. For instance, Fu *et al* [13] proposed and demonstrated a fiber supercapacitor which used commercial pen ink as its active material. To fabricate the supercapacitor, pen ink (active component: carbon graphite nano-particles) is coated on two fiber electrodes by dip-coating. With an insulating spacer wire wrapping around one of the electrodes, the two electrodes are placed closely in parallel and packaged into a plastic tube. A gel-form electrolyte consisting of poly(vinyl alcohol) and sulfuric acid is used. This fiber supercapacitor is highly flexible and features a high linear-capacitance of ~0.504 mF cm^{-1}. Note that this supercapacitor also requires manual insertion of electrode wires into the packaging tube.

Fiber batteries may be fabricated by traditional fiber drawing technique which potentially allows drawing of tens of kilometers of fiber in a single processing step. For example, our group [14] has recently reported fabrication of the flexible and stretchable battery sheets composed of $LiFePO_4$ cathode, $Li_4Ti_5O_{12}$ anode and a solid polyethylene oxide electrolyte as a separator layer. Owing to the presence of solid thermoplastic electrolyte, this battery sheet could be potentially rolled into fiber preforms and then drawn into fibers or thin strips which are directly compatible with the weaving process used in smart textile fabrication. Moreover, we have also demonstrated in [15] that metal wires could be co-drawn with thermoplastic polymers, which implies the possibility of single-step fabrication of traditional galvanic battery cells in the fiber form.

In this paper, we further explore this idea and demonstrate that an aluminum–sodium hypochlorite (Al–NaOCl) fiber battery system could indeed be fabricated by co-drawing metallic electrode wires together with microstructured polymer fiber preform. Experimentally, copper and aluminum wires are chosen to be the electrodes which are codrawn with low-density polyethylene (LDPE) preform to form fiber batteries. NaOCl aqueous solution (bleach) is then filled in the fiber batteries as electrolyte. In this paper we also report some basic electrochemical properties of the Al–NaOCl fiber battery system including open voltage, capacity and internal resistance of the fiber batteries. Due to their flexibility and light weight, the fiber batteries can be woven into a wearable fiber battery textile, or they could be integrated into other 'smart' textiles as power sources. As a proof-of-principle, we then demonstrate several applications of our fiber battery textiles including: lighting up an LED, driving a wireless mouse, and actuating a textile screen with an integrated shape-memory nitinol wire. Among the key advantages of the proposed Al–NaOCl fiber batteries and the corresponding fiber battery textiles, we note ease of fabrication, ease of servicing and integration, as well as simplicity of electrochemistry, broad availability and low cost of the underlying chemical components and high current-carrying capacity.

We would like to stress that the main goal of this paper is not in the detailed understanding of the electrochemistry involved in an Al–NaOCl battery system. Although we do present some results related to basic electrochemical characterization of our Al–NaOCl fiber batteries, these results are by no means complete or exhaustive. The main goal of this paper is rather to demonstrate that using advanced packageing approaches (like fiber drawing), electrochemically simple batteries can be implemented in a slender and flexible fiber form that is suitable for seamless integration into smart textile prototypes.

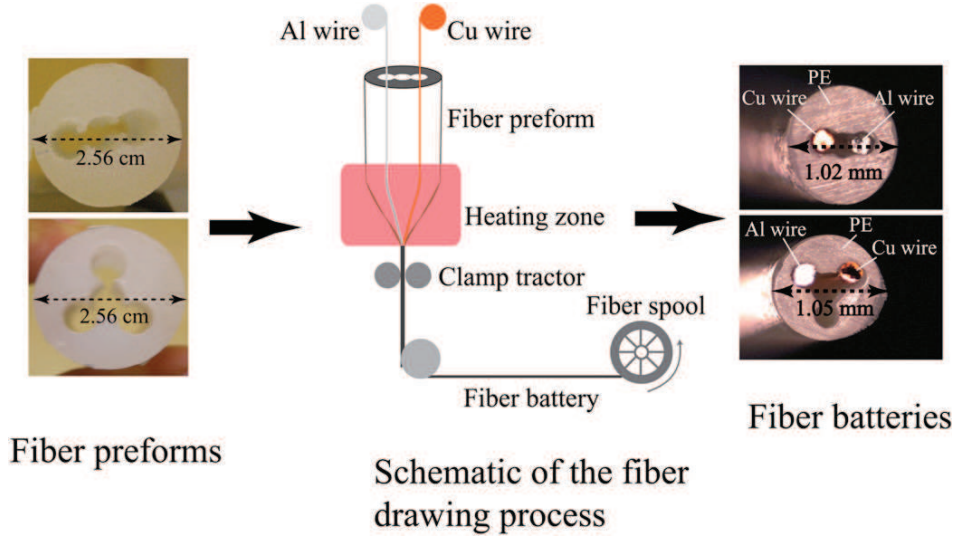

Figure 1. (Left) cross sections of fiber preforms used in the fiber battery fabrication. (Middle) schematic of the fiber drawing process from a preform. (Right) cross sections of the two fiber batteries. The fiber at the top features a three-channel structure, while the fiber at the bottom features a four-channel structure. In each fiber battery, an aluminum wire and a copper wire are immobilized in the two extreme channels of the polyethylene jacket; voids between the two metallic electrodes are filled with electrolyte. The diameter of both fiber batteries is ∼1 mm.

Our paper is structured as follows. Section 2 details fabrication of the fiber battery as well as electrochemical reactions involved in an Al–NaOCl battery system. In section 3, we first study performance of a standard Al–NaOCl galvanic cell (infinite electrolyte) and characterize its internal resistance as a function of the distance between two electrode wires. We then perform electrochemical characterization of the fiber batteries and find that their performance is limited due to a small amount of electrolyte available in the fiber core. The properties of the fiber batteries such as open voltage, short-circuit current, capacity and internal resistance are measured and compared to those of bulk galvanic cells with comparable inter-electrode separation. In section 4, we fabricate several fiber battery textiles and demonstrate three applications of these fiber battery textiles including lighting up an LED, powering a wireless mouse and actuating a nitinol wire. Moreover, we also discuss optimization of the output power of a fiber battery textile by choosing the proper connectivity between the individual fiber batteries. We conclude that via judicious choice of the connectivity topography between the individual fiber batteries one can implement various power plans for the optimal operation of a fiber battery textile power source.

2. Al–NaOCl fiber batteries: fabrication and electrochemistry

Traditional galvanic battery cells, which were discovered centuries ago, still show their robust vitality in the scientific and industrial world because of their ease of operation and simplicity of electrochemistry. Among a large number of galvanic cells, the Al–NaOCl system has been comprehensively studied due to its advantages such as cost-effectiveness, availability of the chemical components and high current-carrying capacity [16, 17].

2.1. Fiber battery fabrication using fiber drawing

In this paper, we demonstrate, for the first time to our knowledge, fabrication of Al–NaOCl fiber batteries using fiber drawing technique. First step in the preparation of a fiber battery is drawing of the polymer jacket that would eventually host two metallic electrodes and a solvent. To do that we prepare a so-called fiber preform by drilling three or four 6 mm diameter interconnected holes in a 2.56 cm diameter LDPE rod (see the left part of figure 1). The rod length can be several tens of centimeters, and the holes are drilled all the way through the LDPE rod. LDPE is chosen as the jacket material because of its good chemical resistance to various aqueous solutions of salts, acids, alkalis, and a large number of organic solvents. The cross sections of two typical fiber battery preforms used in this work are shown in the left part of figure 1. During drawing process (see the middle part of figure 1), plastic preform is placed into the vertical furnace where the temperature is increased above the polymer softening temperature. As a consequence, the preform tip melts, forms a blob that later falls down under the force of gravity, thus creating a slender fiber that can be continuously pulled from the molten perform tip. In actuality, a clamp tractor is used to continuously pull the fiber at a constant speed. The final size of the resultant fibers depends on the parameters used in the drawing process such as fiber drawing speed, temperature distribution in the furnace, preform feeding speed, as well as overpressure used during fiber fabrication. Several kilometers of the fiber battery can be produced in a single drawing process using our research-grade drawing tower. The fiber drawing technique is, to some extent, similar

to the melt-spinning technique frequently used in the traditional textile industry [18]. However, melt-spinning only allows fabrication of simple fibers, while fiber drawing from preforms allows fabrication of fibers with very complex geometrical profiles featuring almost any arrangement of the individual or overlapping holes. Finally, the electrode wires (aluminum wires and copper wires) can be integrated into the fiber battery directly during the drawing process. To do this, the two wires are wrapped around individual tension-adjustable reels installed above the preform (similar to the technique used in [15]). The wires are then passed through the two extreme holes of a preform. During drawing, softened plastic jacket collapses around the wires that are continuously unwound from the bobbins by the clamp tractor.

In figure 1, we show cross sections of the two typical fiber batteries fabricated by fiber drawing. The outer diameters of the fibers after drawing are in the 1–2 mm range (see the right part of figure 1). In each fiber, an aluminum (Al) wire (99.9% pure, from Mcmaster Carr) and a copper (Cu) wire (99.9% pure, from Mcmaster Carr) are immobilized in the extreme channels of the fiber, while the other holes separating the two electrodes are later filled with NaOCl electrolyte using a syringe. The two fibers in figure 1 feature a three-channel structure (top in the right part) and a four-channel structure (bottom in the right part). The four-channel fiber battery accommodates a larger amount of electrolyte solution, thus generally resulting in a higher capacity than the three-channel fiber. For this reason, in the following presentation we mainly use four-channel fiber batteries. Note that unlike conventional galvanic cells in which separators such as porous membranes are normally used to prevent short circuit between two electrodes, our fiber battery immobilizes its electrode wires within the well separated channels, thus preventing the battery from short circuiting. This design simplifies the fiber battery structure and potentially allows a simple fabrication route via a single fiber drawing fabrication step.

2.2. Electrochemical reactions in the Al–NaOCl system

For the Al–NaOCl battery system, the redox potentials, E^0, versus standard hydrogen electrode are described as follows [16, 17]:

$$\text{anode: Al} \rightarrow \text{Al}^{3+} + 3\text{e}^-; \quad E^0 = 1.7\ \text{V}, \tag{1}$$

$$\text{cathode: OCl}^- + \text{H}_2\text{O} + 2\text{e}^- \rightarrow 2\text{OH}^- + \text{Cl}^-; \quad E^0 = 0.81\ \text{V}. \tag{2}$$

Thus, the most typical overall reaction of the fiber battery is:

$$\text{overall reaction: } 2\text{Al} + 3\text{NaOCl} + 3\text{H}_2\text{O} \rightarrow 3\text{Na}^+ + 3\text{Cl}^- + 2\text{Al(OH)}_3 \downarrow . \tag{3}$$

Reactions (1)–(3) demonstrate that the Al–NaOCl system is capable of attaining a theoretical potential of 2.51 V at 'standard chemical state'. At the same time, the following parasitic reaction leads to release of the hydrogen gas during battery operation [17]:

$$\text{parasitic reaction: } 2\text{Al} + 2\text{H}_2\text{O} + 2\text{OH}^- \rightarrow 2\text{AlO}_2^- + 3\text{H}_2 \uparrow . \tag{4}$$

The hydrogen gas generated in the parasitic reaction expels the electrolyte out of the fiber battery, which leads to increase in the battery internal resistance and reduction of the battery capacity. Besides, we note that the product of reaction (3) is $Al(OH)_3$, which is a gel-like precipitant [19] that also increases the battery internal resistance by blocking the ion flow between the two electrodes. The copper wire in this system does not participate in the electrochemical reactions, and it only acts as a current collector and electrocatalyst [17]. In fact, the electrode materials are not limited to the combination of Al and Cu. For instance, Al may be replaced by zinc (Zn) [16] or magnesium [20], while a variety of other metals including nickel, silver, platinum, and their alloys could replace a Cu anode [16, 17]. In this paper, we choose Al and Cu wires as electrodes because of their low cost and availability.

We also note that NaOCl electrolyte by itself does not have a strong spontaneous reaction with an Al wire, since an Al wire normally features an aluminum-oxide passivation layer on its surface, which, to some degree, retards the direct interaction of the Al electrode with bleach. However, long-period immersion of Al wires or foils into the NaOCl solution would cause corrosion and bubbling on the Al surface. Therefore, electrolyte should be preferably introduced into fiber batteries just prior to their utilization.

Finally, all the battery measurements presented in the remainder of the paper are carried out under the standard laboratory conditions (21 °C), and no other additives were used in the electrolyte solution consisting of the deionized water and a purified NaOCl.

3. Electrochemical characterization of the batteries

In this section we perform comparative characterization of the bulk galvanic cells and drawn fiber batteries. Bulk galvanic cells are chosen to have electrode arrangement and size similar to those in the drawn fiber batteries. The only major difference between a bulk galvanic cell and a fiber battery is the amount of electrolyte available for the electrochemical reactions. While in a bulk galvanic cell the electrolyte supply can be considered as infinite, in the fiber battery the quantity of the available electrolyte is limited, thus resulting in the inferior performance of a fiber battery when compared to that of a bulk galvanic cell.

3.1. Bulk battery

We first study performance of a bulk Al–NaOCl galvanic cell (see figure 2). We start by attaching 400 μm diameter, 7 cm long aluminum and copper electrode wires onto the glass plates. The galvanic cell is assembled by placing the two electrodes parallel to each other. The electrodes are then immersed into a 14.5 wt% solution of NaOCl (electrolyte)

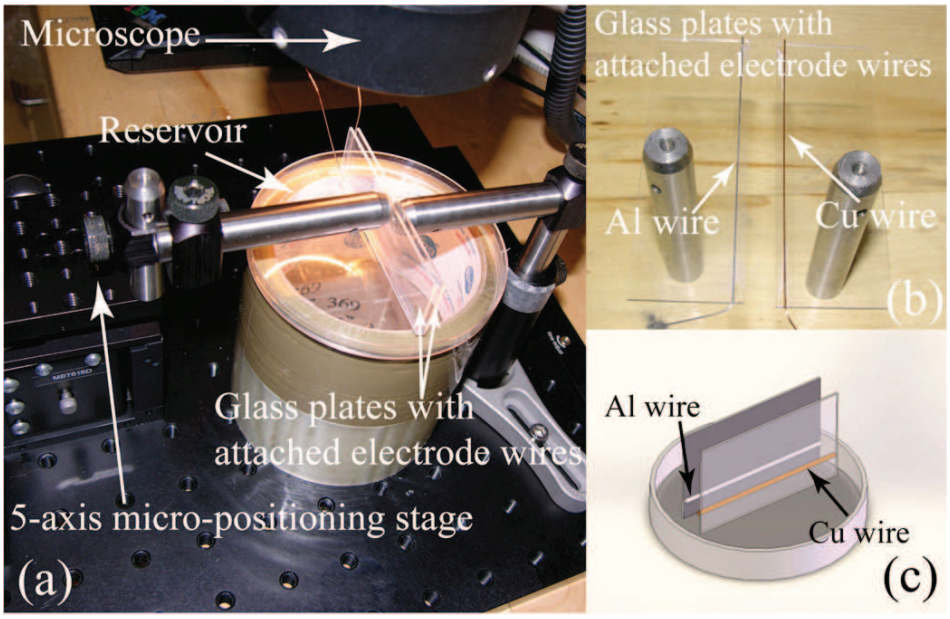

Figure 2. (a) Setup for electrochemical characterization of a bulk Al–NaOCl galvanic cell. (b) Two glass plates with attached electrode wires. (c) Schematic of a bulk battery cell in which an aluminum wire and a copper wire are placed in parallel to each other and then immersed into the electrolyte.

placed inside of a large reservoir. This particular choice of the NaOCl concentration in the solution is determined by the fact that a variety of relatively safe commercial household products are available that feature aqueous solutions of NaOCl with concentrations of up to 15%. Higher concentrations of NaOCl result in moderately and strongly corrosive solutions that could become hazardous for human health at concentrations over 40%. In fact, we have also conducted characterization measurements of the batteries featuring electrolytes with ~5% concentration of NaOCl. Such batteries have performed considerably worse than those containing 14.5% of NaOCl, therefore, we have decided not to detail them in this paper.

During the measurements, the distance between two electrodes is varied from 100 to 900 μm with a 100 μm increment using a 5-axis micropositioning stage and an optical microscope. At each distance, the open-circuit voltage V_b, and the short-circuit current i_b of the bulk battery cell are measured using an electrochemical characterization workstation (IviumStat).This enables us to estimate the internal resistance of the galvanic cells by dividing V_b by i_b as a function of the distance between two electrodes.

The open-circuit voltage of the galvanic cell is measured to be ~1.45–1.5 V, and it is largely independent of the inter-electrode separation. In figure 3, we show time evolution of the short-circuit current in the galvanic cells featuring different inter-electrode separations.

In figure 3 we see that the short-circuit current in the bulk battery cells shows an initial fast decrease from ~200 mA to ~50 mA within the first several minutes of the battery operation. This is followed by a much slower decrease of the cell short-circuit current from ~50 mA to ~20 mA over the next ~20–30 min. Finally, after 30–45 min of operation, the battery fails, which is due to breakage of the thinned aluminum electrode, which is consumed during the battery operation. Since the electrolyte solution in the reservoir could be considered as 'infinite', the reduction of the short-circuit current is mostly caused by the production of the hydrogen bubbles and precipitation of the gel-like $Al(OH)_3$ (see equations (3) and (4)), which essentially reduce the effective area of the electrodes, and, as a consequence, lead to increase in the battery internal resistance.

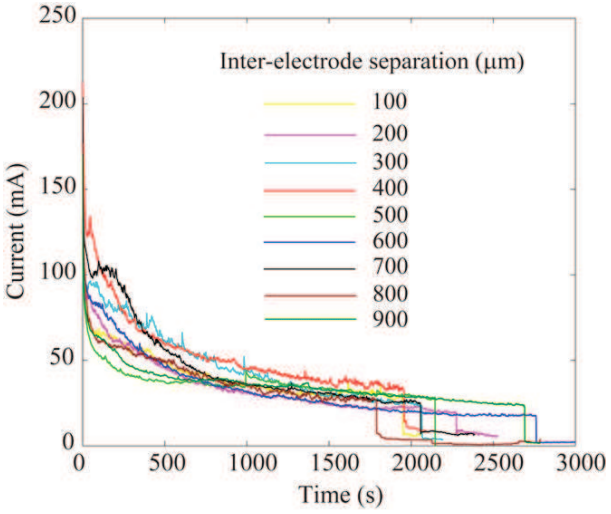

Figure 3. Short-circuit current in the Al–NaOCl galvanic cells. The distance between two electrode wires is varied from 100 to 900 μm with a 100 μm increment. The electrolyte used in the battery cells is 14.5 wt% NaOCl solution.

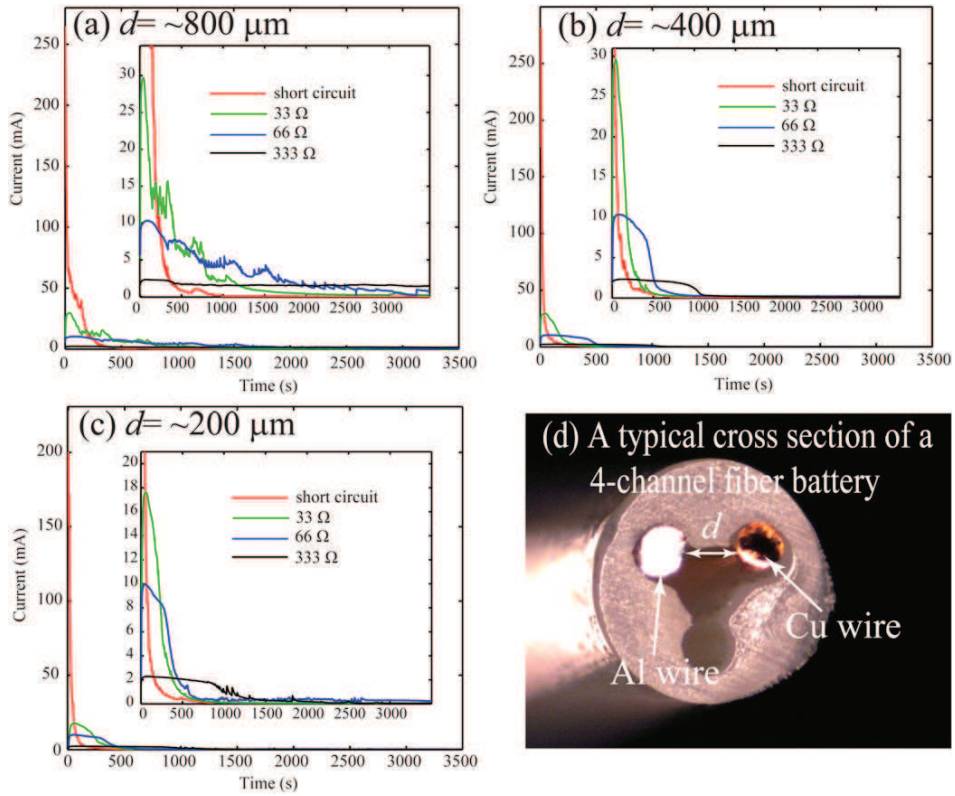

Figure 4. Current generated by three different fiber batteries under different loading conditions. The inter-electrode separations in the four-channel fiber batteries are (a) ~800 μm, (b) ~400 μm, and (c) ~200 μm, respectively. The inset in each figure shows a zoom of the current curves. (d) A typical crossection of a four-channel fiber battery and a definition of the inter-electrode separation d.

Theoretically, the internal resistance R_b of an infinite electrolyte featuring two cylindrical electrodes separated by distance d can be found from basic electrostatics [21]:

$$R_b \approx \frac{1}{\pi L \sigma} \ln\left(\frac{d + 2r_0}{r_0} - 1\right), \tag{5}$$

where σ electrolyte conductivity, L is the length of the electrodes, r_0 is the radius of the wires, d is the distance between two electrode wires (d is defined in figure 4(d)). From equation (5), the internal resistance of a two-electrode-wire battery system is only weakly dependent on the inter-fiber separation, and it should be constant over time assuming constant conductivity of the electrolyte and constant effective area of the wire electrodes. However, in our bulk Al–NaOCl galvanic cells, the internal resistance shows significant changes over time. Moreover, we could not find a simple functional dependence of the cell internal resistance on the inter-electrode separation because of the generation of gas bubbles (see equation (4)) and $Al(OH)_3$ gel precipitation (see equation (3)) during the whole battery discharging process. Particularly, when conducting observations under the microscope, we observe generation of the hydrogen bubbles that initially stick to the Al electrode, thus reducing its active surface and increasing the battery internal resistance. Over time, the coverage of the Al electrode with gas bubbles increases, leading to spontaneous formation of larger bubbles that sometimes leave the electrode, and result in rapid variations in the battery performance. Moreover, $Al(OH)_3$ gel precipitation leads to further reduction of the Al electrode surface and consistent degradation of the battery performance over time. We believe that it is due to uncertainty associated with the random processes of hydrogen bubble formation and gel precipitation on the Al electrode, that we observe pronounced sample-to-sample variations in the battery performance. From figure 3, we estimate that the instantaneous short-circuit current measured in a repeated measurement has variations up to 40% in amplitude. These variations are consistently observed for the measurements of the battery short-circuit current for other batches of batteries with similar geometries. Such variations, in fact, mask the true dependence of the battery properties on the inter-electrode separation, and, therefore, we can only comment on the average properties of the bulk galvanic cells measured in this work. Based on the results presented in figure 3, we estimate that the internal resistivity of the bulk batteries with sub-1 mm inter-electrode separation and 400 μm diameter wire electrodes is ~0.5–2 $\Omega \cdot$m in the first few minutes of battery discharging, while increasing to 2–5 $\Omega \cdot$m closer to the end-life of a battery (30–45 min). We remind the reader that battery resistivity is calculated by multiplying the battery resistance by the electrode length $V_b/i_b \cdot L$. Finally, the linear capacity of

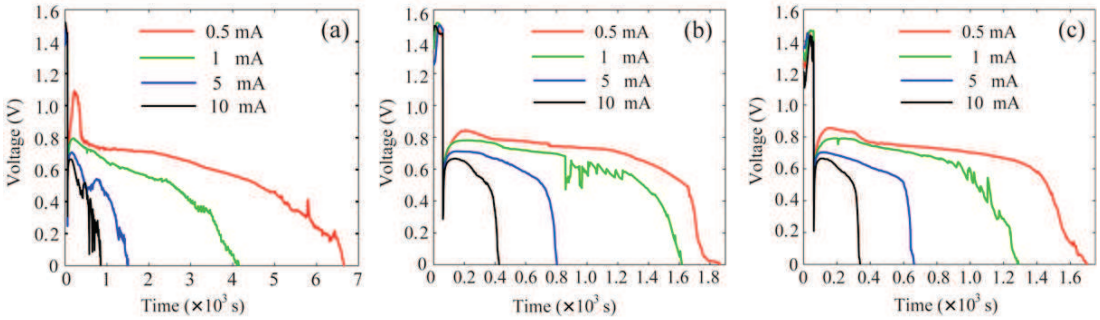

Figure 5. Three fiber batteries (same as in figure 4) discharged with different constant currents. Before discharging each fiber battery is kept as 'open cell' for 60 s.

these bulk battery cells is measured to be 3–4 mAh cm^{-1} till the failure of the battery.

3.2. Fiber battery

In the second batch of experiments, we characterize the performance of three 15 cm long, four-channel (see figure 1(b)) fiber batteries. The three batteries feature different inter-electrode separations of ∼800 μm, ∼400 μm and ∼200 μm. The electrode wires (both Al and Cu wires) inserted into the fibers have a diameter of 400 μm (same diameter as in the case of bulk galvanic cells). A 14.5 wt% NaOCl solution in water is used as an electrolyte, which is introduced into battery using a syringe. The open-circuit voltage of all the fiber batteries is measured to be ∼1.45–1.5 V. We, then, studied battery generated current under different resistive loading conditions, such as: short-circuited battery, resistive load of 33 Ω, 66 Ω and 333 Ω. The time evolution of the current under different loading conditions is measured for ∼1 h by the IviumStat electrochemical characterization workstation with a 15 μA resolution, and the results are presented in figure 4.

Based on the short-circuit current and the open voltage of the fiber batteries, we could estimate the average internal resistivity of these fiber batteries to be ∼0.9–4 $\Omega \cdot$ m, when the fiber batteries are in the first few minutes of discharging. Such a resistivity is comparable to that of a bulk galvanic cell. We note that as it is the case in bulk galvanic cells, the inter-electrode separation has little effect on the resistivity of a fiber battery. During discharge of the fiber batteries, hydrogen bubbles and gel-like $Al(OH)_3$ are continuously generated. In particular, the hydrogen bubbles not only reduce the effective electrode area, but they also cause leakage of the electrolyte solution out of the fiber battery due to very limited internal volume of the fiber channels. Therefore, the short-circuit current of a fiber battery drops much quicker than that of a bulk galvanic cells studied in the previous subsection. Thus, after 10 min discharging, the short-circuit current in all the measured fiber batteries dropped below ∼1 mA. As a consequence of the electrolyte expulsion, the fiber battery capacity is considerably smaller than that of the corresponding bulk galvanic cell, where the principal factor limiting battery capacity is rather a failure of the aluminum wire integrity due to its consumption in the electrochemical reaction. Moreover, similar to the case in bulk battery cells, the instantaneous short-circuit current measured in a repeated measurement is estimated to have a fluctuation of up to 40% in amplitude because of the generation of hydrogen bubbles and $Al(OH)_3$ gel. In figure 4, we also present fiber battery discharge curves under different resistive loads. Thus, with loads of 33 Ω and 66 Ω, a fiber battery could generally provide a current higher than 5 mA for 5–15 min. When using a 333 Ω resistor as a load, a fiber battery could generally discharge at ∼2 mA for more than 15 min. Note that when a fiber battery is loaded with a resistor, its discharging current is much smaller than the short-circuit current, thus resulting in a slower production of hydrogen bubbles and $Al(OH)_3$ gel. Therefore, we estimate that the corresponding fluctuation in the instantaneous current in a repeated measurement is much smaller than 40%.

In order to calculate fiber battery capacities we performed a set of discharge measurements under the constant current condition using the same fibers as in the previous paragraph. Actually, we expect that capacity of a fiber battery should increase for larger inter-electrode separations simply because the volume of electrolyte will be larger in such fibers. In order to measure the capacity of fiber batteries, we use the IviumStat (as a galvanostat) to discharge the batteries at a constant discharging current. Particularly, the fiber batteries are first kept as 'open cells' for 60 s after filling them with electrolyte, and then the fiber batteries are discharged at the constant currents of 0.5, 1, 5 or 10 mA, respectively. The capacity of a fiber battery can then be calculated by integrating the current until the output battery voltage drops to zero.

Based on the result shown in figure 5, we are able to calculate the capacity of each fiber battery discharged with different currents. The capacity of the three fiber batteries are shown in table 1. Besides, in table 1, we also summarize the internal resistivity, electrolyte volume, and specific energy of both the bulk battery cells and fiber battery cells. To analyze the experimental error for the measurements of capacities and specific energy, we repeat five times the constant-current discharging experiments of the fiber battery used in figure 5(b). We find that the measured values for both capacity and specific energy generally show a fluctuation of less than 8% in the repeated measurements.

The main limitation in the operation of our fiber battery is generation of the hydrogen gas. As shown in figure 6, gas

Table 1. Internal resistivity, capacity, electrolyte volume, and specific energy of both the bulk galvanic cells and the fiber batteries studied in this work.

Battery	Initial internal resistivity ($\Omega \cdot$ m) (in the first few minutes of discharge)	Electrolyte volume (μL cm^{-1}) (per 1 cm of fiber length)	Capacity (mAh cm^{-1}) (per 1 cm of fiber length)	Specific energy (Wh g^{-1}) (per 1 g of active material)
Bulk cells	~0.5	∞	3–4 mAh cm^{-1}	—
			0.140 at 10 mA	18.7×10^{-3} at 10 mA
			0.129 at 5 mA	17.8×10^{-3} at 5 mA
Fiber (a)	~0.83	~11.2	0.075 at 1 mA	11.2×10^{-3} at 1 mA
			0.061 at 0.5 mA	10.2×10^{-3} at 0.5 mA
			0.067at 10 mA	11.0×10^{-3} at 10 mA
			0.067 at 5 mA	12.3×10^{-3} at 5 mA
Fiber (b)	~0.80	~6.1	0.029 at 1 mA	5.2×10^{-3} at 1 mA
			0.017 at 0.5 mA	3.3×10^{-3} at 0.5 mA
			0.051 at 10 mA	8.6×10^{-3} at 10 mA
Fiber (c)	~1.12	~5.0	0.055 at 5 mA	9.8×10^{-3} at 5 mA
			0.022 at 1 mA	4.2×10^{-3} at 1 mA
			0.015 at 0.5 mA	3.2×10^{-3} at 0.5 mA

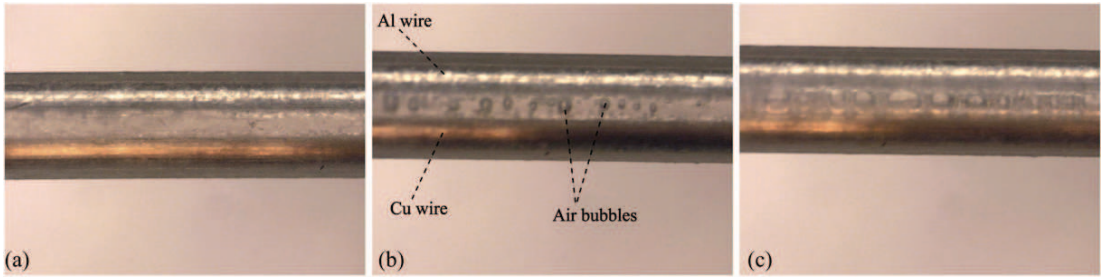

Figure 6. Fiber battery (a) open circuit; (b) short-circuited, after 5 s; (c) short-circuited, after 40 s.

bubbles are generated immediately after the current starts flowing through the battery (figure 6(b)). As a consequence, part of electrolyte is expelled out of the fiber within the first several minutes after discharging (figure 6(c)). We tried to use epoxy to seal both ends of a fiber battery in order to prevent leakage. However, the generation of gas bubbles would considerably increase the internal fluidic pressure of the fiber battery, and eventually damage the sealing. Note that the components and the reaction products involved in the battery reaction are non-hazardous materials. Thus, the leakage of these materials would pose little danger to human wearers or working environments. However, NaOCl, the main component of household and industrial bleach, could whiten the fiber battery textiles or other fabrics, which constitutes the main disadvantage of this NaOCl fiber battery. In principle, leakage of electrolyte may be alleviated by adding certain chemicals into one of the fiber empty channels in order to absorb the hydrogen gas or to convert hydrogen into water through hydrogen–oxygen reaction. However, research on this topic is beyond the scope of this paper.

4. Fiber battery textiles

In this final section we present several examples of fiber battery textiles that are fabricated from individual fiber batteries using a Dobby loom. We demonstrate flexibility of such fiber battery textiles and their versatility as power sources for various applications in lightning, electronics, and actuation. We also discuss the issue of realizing different power plans by using different connection schemes between the individual fiber batteries.

4.1. Lighting up an LED

Due to their small diameter (<2 mm), and flexibility, the developed fiber batteries can be readily woven into a textile. For example, it is possible to weave 200 pieces of the 10 cm long fibers into a 10 cm × 50 cm ribbon. By connecting every two adjacent batteries in series, and then connecting the resulting 100 fiber pairs in parallel, we could fabricate a fiber textile battery with an open voltage of a ~3 V and a total capacity of 0.1 Ah. This fiber battery textile can light up a standard light emitting diode (20 mA at 3 V) for about 5 h. In figure 7, we show an LED lit up by two fiber batteries woven in a textile and connected in series.

4.2. Powering a wireless mouse

Next, we use fiber battery textile as a power supply and a mouse pad for the Logitech M325 wireless mouse with the working voltage and current of 1.5 V and 30 mA, respectively.

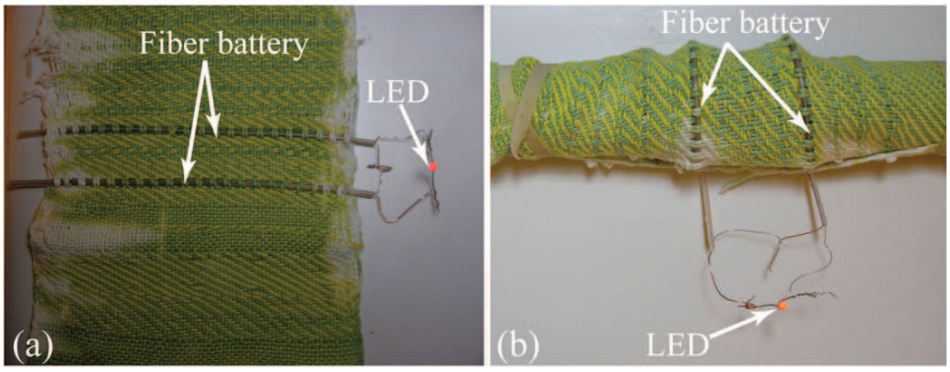

Figure 7. An LED is lit up by two fiber batteries woven in a textile and connected in series. Particularly, in order to demonstrate the flexibility of the fiber battery textile, we wrapped it around a cylindrical rod of 32 mm in diameter as shown in (b).

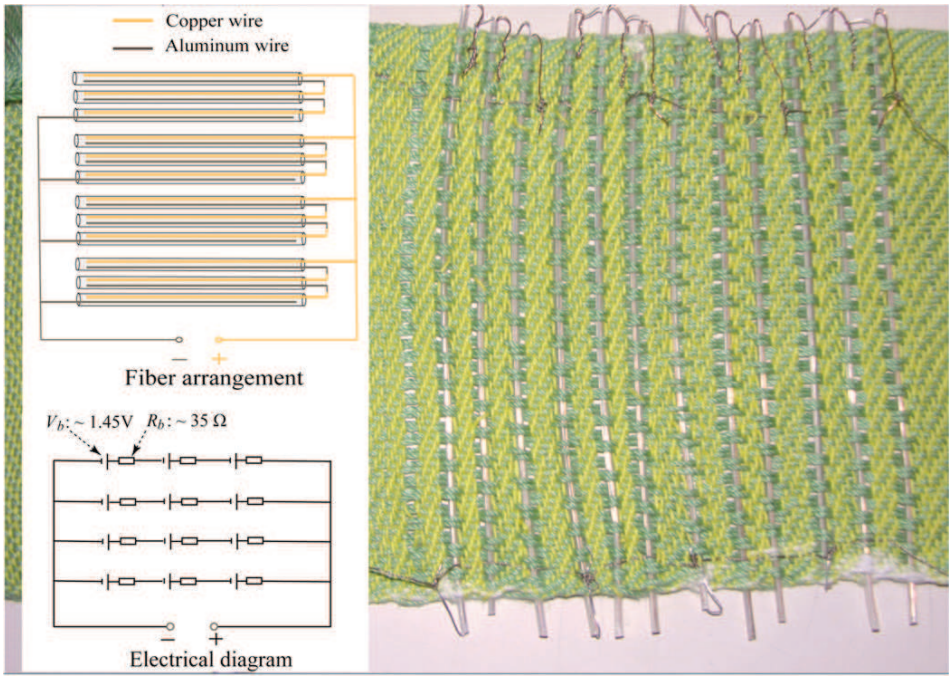

Figure 8. A fiber battery textile works as a power supply and a mouse pad for a wireless mouse. The inserts on the left show schematic of the fiber arrangement and the corresponding electrical diagram. The open voltage of an individual fiber is $V_b \sim 1.45$ V and its internal resistance is $R_b \sim 35\ \Omega$.

Experimentally, we weave 12 fiber batteries into a textile. An individual fiber battery is 15 cm long and it features 400 μm diameter electrodes that are placed at a distance of ~800 μm with respect to each other. The open circuit voltage of an individual fiber battery is $V_b \sim 1.45$ V and its internal resistance is ~35 Ω as estimated from the figure 4(a) (red curve that gives ~40 mA current for the first ~3 min). These fiber batteries are divided into four groups connected in parallel. Each group consists of three fiber batteries connected in series as shown in figure 8. Based on this configuration, we estimate that each fiber battery would provide a current of 5–10 mA, so that the fiber battery textile consisting of four groups in parallel is able to provide a current of 20–40 mA, which could meet the working current of the wireless mouse. Besides, according to the results shown in figure 5, when a fiber battery discharges at a constant current of 5–10 mA, its output voltage is ~0.6 V. Thus, we use three fiber batteries connected in series to ensure the output voltage of this fiber battery textile to be ~1.8 V. We then fill the electrolyte solution of 14.5 wt% NaOCl into each fiber battery using a syringe, and we use this fiber battery textile to power up the wireless mouse. Experimentally, we could power the wireless mouse for up to 10 min. During the experiment, the textile was also deformed in a variety of ways in order to show its flexibility without sacrificing its performance. A detailed video of this experiment is available at the following web site [22].

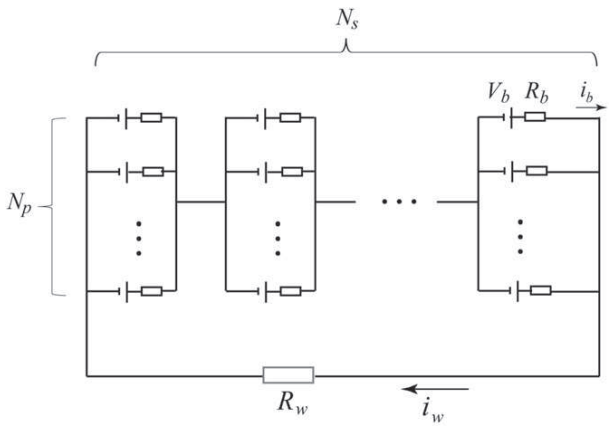

Figure 9. Schematic of a fiber battery textile in which fiber batteries are divided into N_s groups connected in series, and each group consists of N_p fiber batteries connected in parallel. We assume that a single fiber battery has an open voltage of V_b and an internal resistance of R_b. We also assume the current passing through a single fiber to be i_b and the current passing through the load to be i_w. The load is considered to be a simple resistor with resistance R_w.

4.3. Actuating a shape-memory nitinol wire screen

As a final demonstration, we use a fiber battery textile as a power source that allows us to heat and actuate a nitinol wire. We remind the reader that nitinol is a shape memory alloy composed of nickel and titanium. When a nitinol wire is deformed, it could return to its preset shape after heating. Integration of a nitinol wire into a textile could provide dynamic features to the textile, which is of clear benefit to medical and fashion industries. In our experiment a preset shape of a nitinol wire is a spring. We first stretch the spring and sew it to a straight black sheet of fabric (screen). We then heat up the nitinol wire by connecting it to the fiber battery textile. Upon heating over some critical temperature the nitinol wire returns back to its initial shape of a spring, thus contracting the black screen. By disconnecting the nitinol wire from the power source and after cooling the wire, one can again stretch the wire and return the fabric screen into its original form. In what follows, we first detail how to theoretically optimize the connectivity between the individual fiber batteries in a textile to provide the maximized output power (i.e. most efficient heating of the nitinol wire). Then, we experimentally demonstrate using a fiber battery textile with optimized connectivity in order to actuate a fabric screen with an integrated nitinol wire spring.

4.3.1. Optimization of the output power of a fiber battery textile.

When a fiber battery textile is used for actuating of a nitinol wire, the output power of the fiber battery textile needs to be maximized in order to provide the most efficient heating. This requires optimization of the electrical connections between the individual fiber batteries in a textile. In what follows we assume that the total number of the fiber batteries in a textile is N_t. These fiber batteries are then divided into N_s groups connected in series. Each group consists of N_p fiber batteries connected in parallel. This fiber battery textile is then connected to a nitinol wire of resistance R_w (see figure 9). We now perform a theoretical analysis to demonstrate how to optimize the parameters N_s and N_p that maximize the ohmic heating of the nitinol wire.

We consider that a single fiber battery has an open voltage of V_b and an internal resistance of R_b. When electrical resistance R_w is connected to the fiber battery textile, the current (denoted as i_w) passing through the load can be calculated as:

$$\begin{aligned}&\left(V_b - i_b \cdot R_b\right) \cdot N_s = i_w \cdot R_w\\ &i_w = N_p \cdot i_b,\end{aligned} \tag{6}$$

where i_b denotes the current passing through a single fiber battery. From (6), we obtain:

$$i_w = \frac{N_p \cdot N_s \cdot V_b}{N_s \cdot R_b + N_p \cdot R_w}. \tag{7}$$

From (7) we can make several interesting conclusions about performance of the fiber battery textiles depending on the fiber battery connectorization. Thus, connecting all the fiber batteries in parallel ($N_p = N_t,\ N_s = 1$) and using a large enough number of fibers ($N_t \gg R_b/R_w$) would result in a fixed voltage source that would provide stable currents that are inversely proportional to the load resistance:

$$\begin{aligned}&\text{in parallel}\\ &i_w = \frac{V_b}{R_b/N_t + R_w} \underset{N_t\to\infty}{=} \frac{V_b}{R_w},\\ &V_w = i_w \cdot R_w = \frac{V_b R_w}{R_b/N_t + R_w} \underset{N_t\to\infty}{=} V_b.\end{aligned} \tag{8}$$

On the other hand, connecting all the fiber batteries in sequence ($N_p = 1,\ N_s = N_t$) and using a large enough number of fibers ($N_t \gg R_w/R_b$) would result in a fixed current source. If the load resistance is much larger than the internal resistance of an individual fiber battery, this will also result in high voltage drop on the load:

$$\begin{aligned}&\text{in sequence}\\ &i_w = \frac{V_b}{R_b + R_w/N_t} \underset{N_t\to\infty}{=} \frac{V_b}{R_b}\\ &V_w = i_w \cdot R_w = \frac{V_b R_w}{R_b + R_w/N_t} \underset{N_t\to\infty}{=} V_b \frac{R_w}{R_b}.\end{aligned} \tag{9}$$

Returning to the problem of efficient heating of the nitinol wire, Ohmic power loss on the load is given by:

$$\begin{aligned}P = {i_w}^2 \cdot R_w &= \left(\frac{N_p \cdot N_s \cdot V_b}{N_s \cdot R_b + N_p \cdot R_w}\right)^2\\ &\cdot R_w = \left(\frac{N_t \cdot V_b}{N_s \cdot R_b + N_p \cdot R_w}\right)^2 \cdot R_w.\end{aligned} \tag{10}$$

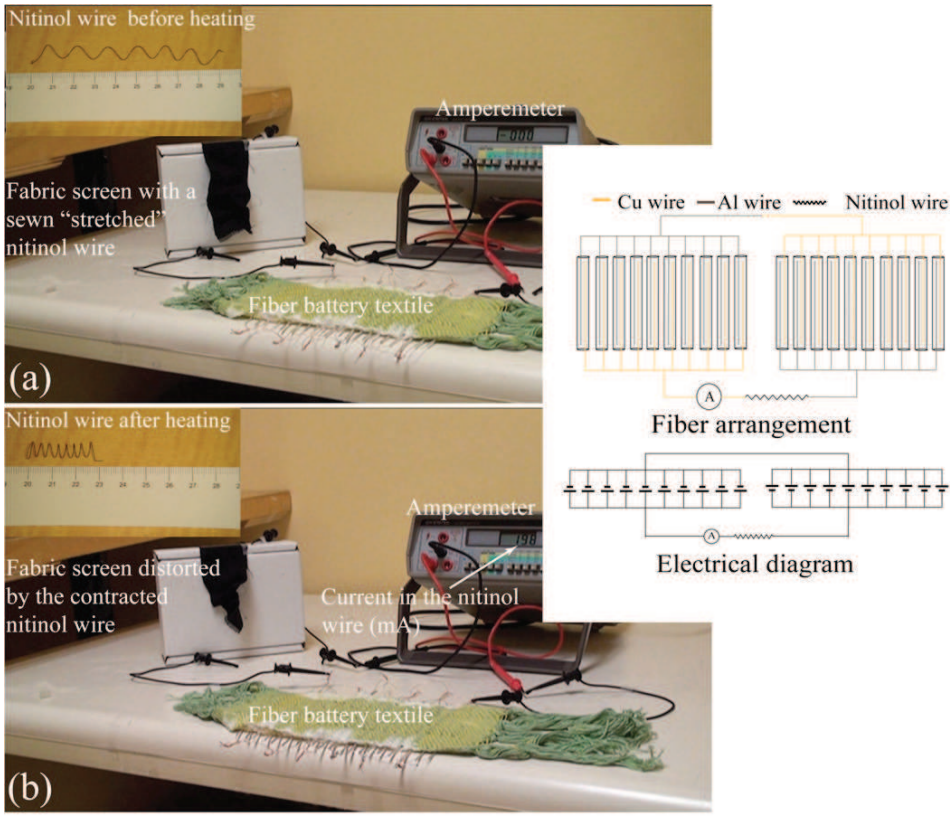

Figure 10. A nitinol wire sewn to a black fabric screen is heated (actuated) using the fiber battery textile. (a) The nitinol wire is first stretched from its programmed spring form and then sewn to a flat fiber screen; (b) the nitinol wire returns to its pre-deformed form (spring) after heating, thus causing the fabric screen to deform. The insert on the right shows the fiber arrangement in the textile and electrical diagram of the fiber battery textile. The two inserts in (a) and (b) show the shape of the nitinol wire before and after heating, respectively.

By solving $\partial P/\partial N_s = 0$ we now find the optimal value N_s^{opt} that maximizes Ohmic loss (heating) in the nitinol wire:

$$N_s^{\text{opt}} = \sqrt{\frac{R_w}{R_b} \cdot N_t}. \tag{11}$$

From section 3.2, we know that the internal resistance of a fiber battery is a dynamic value. Although the initial internal resistance of a 15 cm long fiber battery could be as low as $\sim 7\,\Omega$, it increases to $\sim 40\,\Omega$ after discharging for a few minutes. Therefore, we assume that a fiber battery has an internal resistance less than $40\,\Omega$ for this nitinol wire experiment. Thus, if we use 20 fiber batteries with internal resistance $R_b = 40\,\Omega$ to actuate the nitinol wire with resistance $R_w = 5\,\Omega$, the optimal number of fiber groups connected in series is $N_s^{\text{opt}} = \sqrt{5\Omega/40\Omega \cdot 20} \approx 1.6$. As N_s is integer, in our experiment we take $N_s = 2$.

Finally, we note that the maximal current and the maximal ohmic loss can be found by substituting N_s^{opt} into (7, 10):

$$i_w^{\max} = \frac{\sqrt{N_t} \cdot V_b}{2\sqrt{R_b \cdot R_w}};\ P_{\max} = \frac{N_t \cdot V_b^2}{4R_b}. \tag{12}$$

4.3.2. Experiment with nitinol wire actuation. Experimentally, we use a 15 cm long, 0.25 mm diameter nitinol wire with the transformation temperature of $\sim 35\,^{\circ}\text{C}$ (from Kellog's Research Labs). The electrical resistance of the wire is measured to be $\sim 5\,\Omega$. We first train the nitinol wire into a spring shape by winding a nitinol wire around a screw and heating the wire at 375 °C for 40 min. The trained nitinol wire is then stretched and sewed to a fabric screen. As a power source we weave a fiber battery textile consisting of 20 fiber batteries. An individual fiber battery has a length of ~15 cm. Based on the optimization in section 4.3.1, we divide all the fiber batteries into two groups that are connected in series. Each group consists of ten fiber batteries connected in parallel. Such an arrangement ensures efficient heating of the nitinol wire, which is important for efficient actuation. The electrolyte of 14.5 wt% NaOCl is then manually introduced into each fiber battery using a syringe. Experimentally, the fiber battery textile with this optimized fiber arrangement could provide an overall current of ~200 mA and efficient heating. Heating above the transformation temperature recovers the nitinol wire into its initial spring shape, thus contracting the black screen (see figure 10). To reset the experiment one simply disconnects the textile power source

and stretches the fiber screen back to its flat shape. The experiment can be repeated many times. A detailed video of the experiment is available at the following web site [23].

5. Conclusion

In summary, we demonstrate fabrication of the flexible Al–NaOCl galvanic fiber batteries for smart textile applications. The fiber battery features Al and Cu wire electrodes placed in a microstructured LDPE jacket with some of the holes filled with NaOCl electrolyte. The performance of the fiber battery is studied and compared to that of a bulk galvanic cell of the same type. We note that for a bulk galvanic cell with 'infinite' electrolyte, the discharging current is mainly limited by the increasing internal resistance due to the generation of hydrogen bubbles and $Al(OH)_3$ precipitate on the electrode surfaces. Throughout its discharging process, the internal resistivity of a bulk battery is typically smaller than $5\,\Omega\cdot$m. The linear capacity of the bulk galvanic cells is measured to be 3–4 mAh cm^{-1}, and the failure mode of the battery is breakage of the aluminum wire due to its consumption in the electrochemical reaction. As to the fiber battery with 'finite' electrolyte, its discharging current decreases much more rapidly as compared to that of a bulk battery. The production of hydrogen bubbles not only increases the internal resistance of the battery, but also causes considerable leakage of the electrolyte from the fiber channels, thus strongly reducing its capacity. We experimentally measure the linear capacity of a fiber battery to be $\sim 10^{-2}$–10^{-1} mAh cm^{-1}. Capacity is found to be a sensitive function of the electrolyte volume available in the fiber channels, resulting in the higher capacities for fibers with larger electrolyte volumes. The specific energy of the fiber battery is typically in the range of 3–20 mWh g^{-1}, and is dependent on the discharging current as well as the fiber internal volume. Finally, we demonstrate several energy-storing fiber battery textile prototypes that are used to light up an LED, to drive a wireless mouse and to actuate a nitinol wire attached to a fabric screen. Moreover, we discuss optimization of the textile electrical circuitry (inter-fiber connections) in order to enhance the fiber battery textile performance. We note that the main challenge of this technique is that the leakage of the electrolyte during battery discharging would degrade the fiber battery performance and may cause contamination of the textile fabric. This problem may be alleviated by adding certain chemicals into the fiber battery empty channels in order to absorb the hydrogen gas or to convert hydrogen into water. The principal advantages of the presented fiber batteries include: light weight, ease of fabrication, high flexibility, non-hazardous battery chemicals, and inexpensive and easily available materials used in the battery design. Because of these important advantages, we believe that the Al–NaOCl fiber batteries and power textiles based on such fiber batteries could find their application in the smart textile industry.

Acknowledgments

The authors would like to acknowledge Fort Wayne Metals Inc. for providing body-temperature nitinol-wire samples for our research project. The authors also thank Prof Joanna Berzowska from Concordia University for providing high-temperature nitinol-wire samples and offering many valuable suggestions for handling of such wires. We also acknowledge the financial support of this project by the NSERC strategic grant STPGP447326-13.

References

[1] Hu J, Meng H, Li G and Ibekwe S I 2012 A review of stimuli-responsive polymers for smart textile applications *Smart Mater. Struct.* **21** 053001
[2] Cherenack K and Pieterson L V 2012 Smart textiles: challenges and opportunities *J. Appl. Phys.* **112** 091301
[3] Windmiller J R and Wang J 2012 Wearable electrochemical sensors and biosensors: a review *Electroanalysis* **25** 29–46
[4] Gorgutsa S, Gu J F and Skorobogatiy M 2012 A woven 2D touchpad sensor and a 1D slide sensor using soft capacitor fibers *Smart Mater. Struct.* **21** 015010
[5] Neudecker B J, Benson M H and Emerson B K 2003 Power fibers: thin-film batteries on fiber substrates *14th Int. Conf. on Composite Materials (ICCM 14)* (San Diego, CA: Society of Manufacturing Engineers)
[6] Wang J, Too C O and Wallace G G 2005 A highly flexible polymer fibre battery *J. Power Sources* **150** 223–8
[7] Wang J, Wang C Y, Too C O and Wallace G G 2006 Highly-flexible fibre battery incorporating polypyrrole cathode and carbon nanotubes anode *J. Power Sources* **161** 1458–62
[8] Kwon Y H *et al* 2012 Cable-type flexible lithium ion battery based on hollow multi-helix electrodes *Adv. Mater.* **24** 5192–7
[9] Ren J, Zhang Y, Bai W, Chen X, Zhang Z, Fang X, Weng W, Wang Y and Peng H 2014 Elastic and wearable wire-shaped lithium-ion battery with high electrochemical performance *Angew. Chem.* **53** 1–7
[10] Weng W, Sun Q, Zhang Y, Lin H, Ren J, Lu X, Wang M and Peng H 2014 Winding aligned carbon nanotube composite yarns into coaxial fiber full batteries with high performances *Nano lett.* **14** 3432–8
[11] Kim J-K, Scheers J, Ryu H-S, Ahn J-H, Nam T-H, Kim K-W, Ahn H-J, Cho G-B and Jacobsson P 2014 A layer-built rechargeable lithium ribbon-type battery for high energy density textile battery applications *J. Mater. Chem.* A **2** 1774–80
[12] Yu X, Fu Y, Cai X, Kafafy H, Wu H, Peng M, Hou S, Lv Z, Ye S and Zou D 2013 Flexible fiber-type zinc–carbon battery based on carbon fiber electrodes *Nano Energy* **2** 1242–8
[13] Fu Y, Cai X, Wu H, Lv Z, Hou S, Peng M, Yu X and Zou D 2012 Fiber supercapacitors utilizing pen ink for flexible/wearable energy storage *Adv. Mater.* **24** 5713–8
[14] Liu Y, Gorgutsa S, Santato C and Skorobogatiy M 2012 Flexible, solid electrolyte-based lithium battery composed of $LiFePO_4$ cathode and $Li_4Ti_5O_{12}$ anode for applications in smart textiles *J. Electrochem. Soc.* **159** A349–56
[15] Gu J F, Gorgutsa S and Skorobogatiy M 2010 Soft capacitor fibers using conductive polymers for electronic textiles *Smart Mater. Struct.* **19** 115006
[16] Cardenas-Valencia A M, Biver C J and Lanebrake L 2007 Reserve, thin form-factor, hypochlorite-based cells for powering portable systems: manufacture (including MEMS processes), performance and characterization *J. Power Sources* **166** 273

[17] Medeiros M G and Zoski C G 1998 Investigation of a sodium hypochlorite catholyte for an aluminum aqueous battery system *J. Phys. Chem.* B **102** 9908
[18] Gupta V B and Kothari V K (ed) 1997 *Manufactured Fiber Technology* (Berlin: Springer) pp 67–97
[19] Serna C J, White J L and Hem L S 1997 Anion–aluminum hydroxide gel interactions *Soil Sci. Soc. Am. J.* **41** 1009
[20] Abner B 1996 Cells with sodium hypochlorite or chlorite and anodes of magnesium or aluminum *J. Electrochem. Soc.* **143** 3133–8
[21] www.mosaic-industries.com/embedded-systems/instrumentation/conductivity-meter/two-electrode-cell-constant
[22] www.youtube.com/watch?v=bre3_EGAGlg www.groupes.polymtl.ca/photonics/textile_energy_storage/Textile_battery_powering_mouse.wmv
[23] www.youtube.com/watch?v=oQwaSHBpgT8 www.groupes.polymtl.ca/photonics/textile_energy_storage/Textile_battery_activating_nitonol_wire.wmv